Human Molecular Genetics, 2016, Vol. 25, No. 22 4951–4961

doi: 10.1093/hmg/ddw318
Advance Access Publication Date: 16 September 2016
Original Article

ORIGINAL ARTICLE

Independent variability of microtubule perturbations associated with dystrophinopathy

Joseph J. Belanto[1], John T. Olthoff[1], Tara L. Mader[2], Christopher M. Chamberlain[1], D'anna M. Nelson[1], Preston M. McCourt[1], Dana M. Talsness[1], Gregg G. Gundersen[3], Dawn A. Lowe[2] and James M. Ervasti[1,*]

[1]Department of Biochemistry, Molecular Biology, and Biophysics, and Program in Molecular, Cellular, Developmental Biology, and Genetics, University of Minnesota – Twin Cities, Minneapolis, MN 55455, USA [2]Programs in Rehabilitation Science and Physical Therapy, Department of Physical Medicine and Rehabilitation, University of Minnesota – Twin Cities, Minneapolis, MN 55455, USA and [3]Department of Pathology & Cell Biology, Columbia University, New York, NY 10032, USA

*To whom correspondence should be addressed at: James M. Ervasti, Tel: (612) 626-6517; Fax: (612) 625-2163; E-mail: jervasti@umn.edu

Abstract

Absence of the protein dystrophin causes Duchenne muscular dystrophy. Dystrophin directly binds to microtubules *in vitro*, and its absence *in vivo* correlates with disorganization of the subsarcolemmal microtubule lattice, increased detyrosination of α-tubulin, and altered redox signaling. We previously demonstrated that the dystrophin homologue utrophin neither binds microtubules *in vitro* nor rescues microtubule lattice organization when overexpressed in muscles of dystrophin-deficient *mdx* mice. Here, we fine-mapped the dystrophin domain necessary for microtubule binding to spectrin-like repeats 20–22. We show that transgenic *mdx* mice expressing a full-length dystrophin/utrophin chimera completely lacking microtubule binding activity are surprisingly rescued for all measured dystrophic phenotypes, including full restoration of microtubule lattice organization. Conversely, despite the presence of dystrophin at the sarcolemma, β-sarcoglycan-deficient skeletal muscle presents with a disorganized and densified microtubule lattice. Finally, we show that the levels of α-tubulin detyrosination remain significantly elevated to that of *mdx* levels in transgenic *mdx* mice expressing nearly full-length dystrophin. Our results demonstrate that the microtubule-associated perturbations of *mdx* muscle are distinct, separable, and can vary independently from other parameters previously ascribed to dystrophin deficiency.

Introduction

Dystrophin is a 427-kDa cytoplasmic protein predominantly expressed in striated muscle (1). Mutations in dystrophin which abolish expression or reduce its functionality lead to Duchenne muscular dystrophy (DMD) or Becker muscular dystrophy, a milder form of the disease (2). Approximately one in every 4000 boys is born with DMD (3), and each of them will inevitably become wheelchair-bound and succumb to fatal cardiac arrest or respiratory failure mainly during their twenties, with an increasing percentage reaching their thirties (4). Current treatment is limited to ventilatory support, which prolongs life, and corticosteroids, which also provide benefit, but can cause serious side effects (5,6).

Received: July 7, 2016. **Revised:** August 15, 2016. **Accepted:** September 12, 2016

In healthy skeletal muscle, dystrophin is enriched at subsarcolemmal protein assemblies known as costameres, where it couples actin and intermediate filaments to a membrane-associated glycoprotein complex (7). In addition, dystrophin directly binds microtubules (8,9), suggesting it may play a role in organizing them into a rectilinear lattice beneath the sarcolemma. The microtubule lattice becomes disorganized when dystrophin expression is ablated as in the *mdx* mouse (8–10) or when dystrophin protein is absent from costameres due to perturbations in other proteins that are required for proper costameric localization of dystrophin, such as ankyrin-B, ankyrin-G, β2-spectrin, dynactin-4 and obscurin (11–13).

Available studies reveal that microtubules are essential in skeletal muscle for myotube formation (14–16) whereas microtubule organization is important for proper Golgi localization in adult skeletal muscle fibers (17,18). In addition, it has been shown that post-translational modification of the microtubule network via detyrosination of α-tubulin in *mdx* cardiac and skeletal muscle contributes to increased production of reactive oxygen species and aberrant calcium regulation (19–21). Previously, we showed that disorganization and/or densification of the microtubule lattice correlates with a decrease in skeletal muscle torque production following eccentric contraction-induced injury (9). However, the relative contributions of microtubule post-translational modification, lattice disorganization and densification to the dystrophic phenotype remain to be determined for both *mdx* mice and human DMD patients.

To further understand the physiologic role of the dystrophin/microtubule interaction and its importance for the molecular pathogenesis of dystrophinopathy, we biochemically mapped the minimal domain within dystrophin necessary for microtubule binding. We previously showed that the dystrophin homologue utrophin neither binds microtubules *in vitro*, nor does it restore microtubule lattice organization when overexpressed in the dystrophin-deficient *mdx* mouse (9). Here, we show that *in vivo* expression of a dystrophin/utrophin chimera lacking *in vitro* microtubule binding activity ameliorates all measured aspects of the *mdx* mouse phenotype, including microtubule lattice organization. Our results demonstrate that the *in vitro* microtubule binding and *in vivo* microtubule organizing functions of dystrophin are independent and separable activities. Furthermore, several microtubule-associated abnormalities of *mdx* muscle including organization, densification and detyrosination vary independently from each other and do not consistently correlate with other well established dystrophy phenotypes.

Results

Based on our previous study (9), we hypothesized that the *in vitro* microtubule binding domain of dystrophin lies within spectrin-like repeats 20–24. Since utrophin lacks microtubule binding activity (9), we attempted to further define the minimal microtubule binding domain in dystrophin by analyzing dystrophin/utrophin hybrid constructs in which varying numbers of homologous utrophin repeats were substituted into dystrophin (Supplementary Material, Fig. S1A). Given the highly similar microtubule binding activities of dystrophin and Dp260 (9), Dp260 was chosen as a template over full-length dystrophin due to its smaller size, ease of cloning and higher protein expression. The exchange of dystrophin repeats 23 and/or 24 for utrophin repeats 21 and/or 22 (Dp260 R24$_{Utr}$ and R23-24$_{Utr}$) did not affect microtubule binding activity (Supplementary Material, Fig. S1A). However, substitution of dystrophin repeat 20 for utrophin repeat 18 (Dp260 R20$_{Utr}$) resulted in a measureable decrease in microtubule binding affinity, similar to that of the substitution of repeats 22–24 with utrophin repeats 20–22 (Dp260 R22–24$_{Utr}$). Moreover, the substitution of two or all repeats within the region of dystrophin repeats 20–22 with utrophin repeats 18–20 (Dp260 R20–21$_{Utr}$, R20–22$_{Utr}$, R20–23$_{Utr}$, R21–24$_{Utr}$ and R20–24$_{Utr}$) resulted in complete loss of specific *in vitro* microtubule binding activity (Supplementary Material, Fig. S1A and Table S1).

To verify that no single repeat within repeats 20–22 is individually responsible for microtubule binding, we analyzed multiple Dp260 constructs deleted for individual spectrin-like repeats 20–24, or hinges 3 or 4 exchanged for the homologous utrophin hinges (Supplementary Material, Table S1). Deletion of each individual repeat from repeat 20 to repeat 24 or swapping of hinge 3 or 4 for the homologous hinge from utrophin did not appreciably impair the microtubule binding activity of Dp260 (Supplementary Material, Table S1). These data indicate that no single repeat within repeats 20–24 is individually responsible for the microtubule binding activity of dystrophin and that neither hinge 3 nor hinge 4 contributes to microtubule binding activity. Taken together, these data indicate that dystrophin repeats 20–22 comprise the minimal region of dystrophin necessary for binding microtubules *in vitro*.

To confirm the results observed with internal deletion constructs (9) and in Dp260/utrophin hybrids (Supplementary Material, Fig. S1A), we analyzed a full-length dystrophin construct in which repeats 20–24 were replaced with the homologous repeats 18–22 of utrophin, as well as a utrophin construct where repeats 18–22 were substituted with dystrophin repeats 20–24 (Fig. 1A–C). As expected, insertion of utrophin repeats 18–22 into Dys R20–24$_{Utr}$ conferred a loss of microtubule binding function, corroborating the lack of microtubule binding we observed for Dp260 R20–24$_{Utr}$ (Fig. 1). Interestingly, constructs encoding only dystrophin repeats 20–22 or 20–24 did not bind microtubules (Supplementary Material, Fig. S1B and C) while insertion of dystrophin repeats 20–24 failed to confer a gain of microtubule binding function to Utr R18–22$_{Dys}$ (Fig. 1A–C). Collectively, our data suggest that dystrophin repeats 20–22 are necessary for direct microtubule binding by dystrophin but are not sufficient to directly bind microtubules in isolation or even within the context of utrophin.

To determine the functional importance of microtubule binding by dystrophin repeats 20–22, we utilized the full-length dystrophin/utrophin hybrid Dys 20–24$_{Utr}$ to create a transgene under the control of the human skeletal α-actin (HSA) promoter, which is expressed solely in skeletal muscle (Fig. 2A). Transgenic founder mice were crossed onto the *mdx* background and named Dys$^{\Delta MTB}$-*mdx* mice. In Dys$^{\Delta MTB}$-*mdx* mice, Dys 20–24$_{Utr}$ is expressed at ∼2-fold above the endogenous dystrophin levels observed in WT mice (Fig. 2B and C). Dys$^{\Delta MTB}$-*mdx* mice display WT levels of utrophin, and α-tubulin (Fig. 2B and C), both of which are significantly elevated in *mdx* mice (8,19,20,22). In addition, Dys$^{\Delta MTB}$-*mdx* mice display incorporation of Dys 20–24$_{Utr}$ into a biochemically-stable dystrophin–glycoprotein complex, indicating that it is forming the proper structure within skeletal muscle (Fig. 2D).

Immunofluorescence analyses on isolated quadriceps muscles from WT, *mdx* and Dys$^{\Delta MTB}$-*mdx* mice verify that Dys 20–24$_{Utr}$ is correctly localized to the sarcolemma and restores localization of the dystroglycans, sarcoglycans, dystrobrevin and syntrophin, all of which are either reduced or absent at the *mdx* sarcolemma (Fig. 3). In addition, the increased localization of utrophin at the sarcolemma of the *mdx* mouse is reduced to WT levels in the Dys$^{\Delta MTB}$-*mdx* mouse, corroborating our western

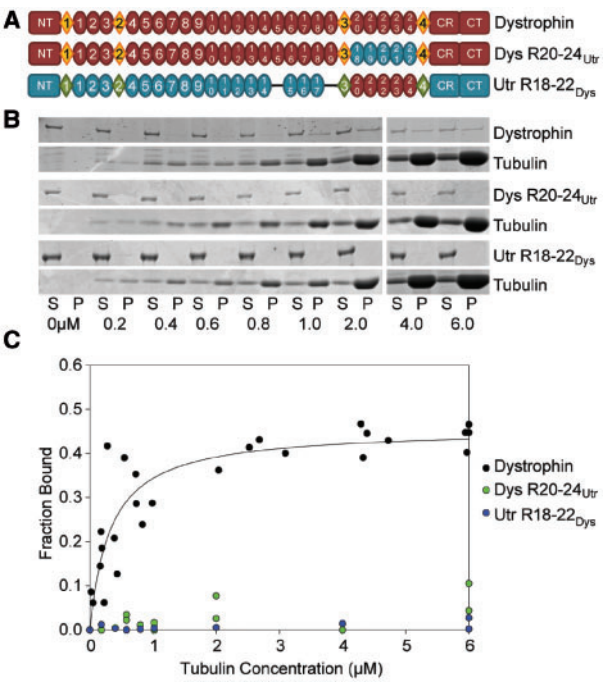

Figure 1. Domain structure and microtubule binding properties of dystrophin/utrophin hybrid constructs. (**A**) Schematic representation of full-length dystrophin and utrophin hybrid constructs used in this study. Ovals represent spectrin-like repeats, diamonds represent hinge regions. NT, N-terminus; CR, cysteine-rich domain; CT, C-terminus. Blue ovals represent portions of utrophin swapped into dystrophin. Red ovals represent dystrophin repeats swapped into utrophin. (**B**) Representative coomassie blue stained SDS-PAGE microtubule cosedimentation gels for dystrophin, Dys 20–24$_{Utr}$, and Utr 18–22$_{Dys}$. S, supernatant (fraction not bound to microtubules); P, pellet (fraction bound to microtubules). Tubulin dimer concentration is listed below each pair of lanes. (**C**) Microtubule binding curves. Substituting dystrophin repeats 20–24 for utrophin repeats 18–22 ablates-specific microtubule binding. However, substituting utrophin repeats 18–22 for dystrophin repeats 20–24 does not confer microtubule binding to utrophin. Full-length dystrophin data was previously published and shown here for reference (9).

blot findings (Fig. 2B). Moreover, histologic assessments of Dys$^{\Delta MTB}$-*mdx* muscle were similar to that of WT muscle (Supplementary Material, Fig. S2A and B). Dys$^{\Delta MTB}$-*mdx* muscle also retains the contiguous neuromuscular junction morphology of WT muscle rather than the fragmented morphology typically observed in the *mdx* mouse (Supplementary Material, Fig. S2C). Taken together, these data indicate that transgenically expressed Dys 20–24$_{Utr}$ correctly localizes within Dys$^{\Delta MTB}$-*mdx* skeletal muscle tissue and properly associates into the dystrophin–glycoprotein complex.

After establishing restoration of the dystrophin–glycoprotein complex in muscle from Dys$^{\Delta MTB}$-*mdx* mice, we quantitatively assessed the morphology of the subsarcolemmal microtubule lattice. Intriguingly, the microtubule lattice of the Dys$^{\Delta MTB}$-*mdx* mouse appeared to be completely rescued from the disorganized and densified microtubule morphology observed in the *mdx* mouse (Fig. 4A). Quantitative analysis of the microtubule lattice revealed that Dys$^{\Delta MTB}$-*mdx* exhibited microtubule density (Fig. 4B) and directionality (Fig. 4C) parameters that were not different from WT muscle, but were significantly different from muscle of non-transgenic *mdx* littermates.

Because our microtubule imaging data of Dys$^{\Delta MTB}$-*mdx* muscle demonstrated a clear separation between the *in vitro* microtubule binding and *in vivo* organizing functions of dystrophin, we investigated whether sarcolemmal dystrophin expression is sufficient for normal microtubule lattice organization in a different model of dystrophy. The mouse lacking β-sarcoglycan (*Sgcb*$^{-/-}$) has a perturbed dystrophin–glycoprotein complex yet expresses WT levels of dystrophin (23,24). *Sgcb*$^{-/-}$ muscle retains the dystroglycans and dystrophin at the sarcolemma, but is lacking the entire sarcoglycan complex due to the absence of the beta subunit. In addition, utrophin is retained at WT levels in *Sgcb*$^{-/-}$ muscle (23,24). Thus, loss of β-sarcoglycan models muscular dystrophy caused by defects in the dystrophin–glycoprotein complex in a manner distinct from the *mdx* mouse. Surprisingly, *Sgcb*$^{-/-}$ muscle displayed a highly densified and disorganized microtubule lattice quantitatively similar to *mdx* muscle (Fig. 4A–C) despite the retention of sarcolemmal dystrophin (23,24). These data indicate that subsarcolemmal microtubule lattice organization is not solely regulated by dystrophin. While it is possible that the sarcoglycan complex may serve as a second important microtubule binding site in the dystrophin–glycoprotein complex, we find that equivalent amounts of α-tubulin co-purify in WGA-enriched fractions from WT and *Sgcb*$^{-/-}$ muscle (Supplementary Material, Fig. S3).

Transgenic utrophin expression in *mdx* muscle fails to fully correct all behavioral and physiological parameters of dystrophy that have been measured (9). Therefore, we measured each of these same parameters in the Dys$^{\Delta MTB}$-*mdx* and *Sgcb*$^{-/-}$ mice. Cage activity after mild exercise (25) revealed that Dys$^{\Delta MTB}$-*mdx* mice performed like WT animals while their non-transgenic littermates and *Sgcb*$^{-/-}$ mice displayed *mdx* levels of inactivity (Fig. 5A). To assess the effects of eccentric contraction on force production (26), we measured both the loss of torque in the anterior crural muscles *in vivo* (Fig. 5B) and loss of force in isolated EDL muscles *ex vivo* (Fig. 5C) in response to a series of eccentric contractions. In both assays, Dys$^{\Delta MTB}$-*mdx* mice showed minimal torque and force losses not different from WT mice. In addition, they performed significantly better than their non-transgenic littermates and *Sgcb*$^{-/-}$ mice, which in turn performed significantly better than *mdx* mice in the *ex vivo* isolated EDL assays. All other physiological measures of isolated EDL muscle function in the Dys$^{\Delta MTB}$-*mdx* mouse were not different from WT (Table 1) while the *Sgcb*$^{-/-}$ muscle performed most similarly to *mdx* muscle. These data collectively indicate that the Dys$^{\Delta MTB}$-*mdx* mouse is fully corrected for all measured *mdx* phenotypes.

Recent studies support a causal relationship between α-tubulin detyrosination and increased expression of the intermediate filament protein desmin with increased production of reactive oxygen species and aberrant calcium regulation in *mdx* skeletal and cardiac muscle (19–21,27). Therefore, we performed quantitative western blot analysis for α-tubulin detyrosination and desmin in skeletal muscle from WT, *mdx*, Dys$^{\Delta MTB}$-*mdx*, Fiona-*mdx*, Dys$^{\Delta 71\text{-}78}$-*mdx* and *Sgcb*$^{-/-}$ mice (Fig. 6A and B). The Fiona-*mdx* mouse model expresses full-length utrophin (28), whereas the Dys$^{\Delta 71\text{-}78}$-*mdx* mouse model expresses nearly full-length dystrophin lacking only a portion of the unstructured C-terminus encoded by exons 71–78 (29), both under control of the HSA promoter. We have used the Dys$^{\Delta 71\text{-}78}$-*mdx* mouse model in previous studies (9) because it stood as the most phenotypically rescued transgenic *mdx* model available. Of the six mouse lines analyzed, *mdx*, Dys$^{\Delta 71\text{-}78}$-*mdx*, and *Sgcb*$^{-/-}$ all showed significantly increased levels of detyrosinated α-tubulin and desmin immunoreactivity (Fig. 6A and B). The high levels of detyrosinated α-tubulin and desmin immunoreactivity in Dys$^{\Delta 71\text{–}78}$-*mdx* muscle is rather counterintuitive since this line is corrected for all measured phenotypes of dystrophy with the exception of

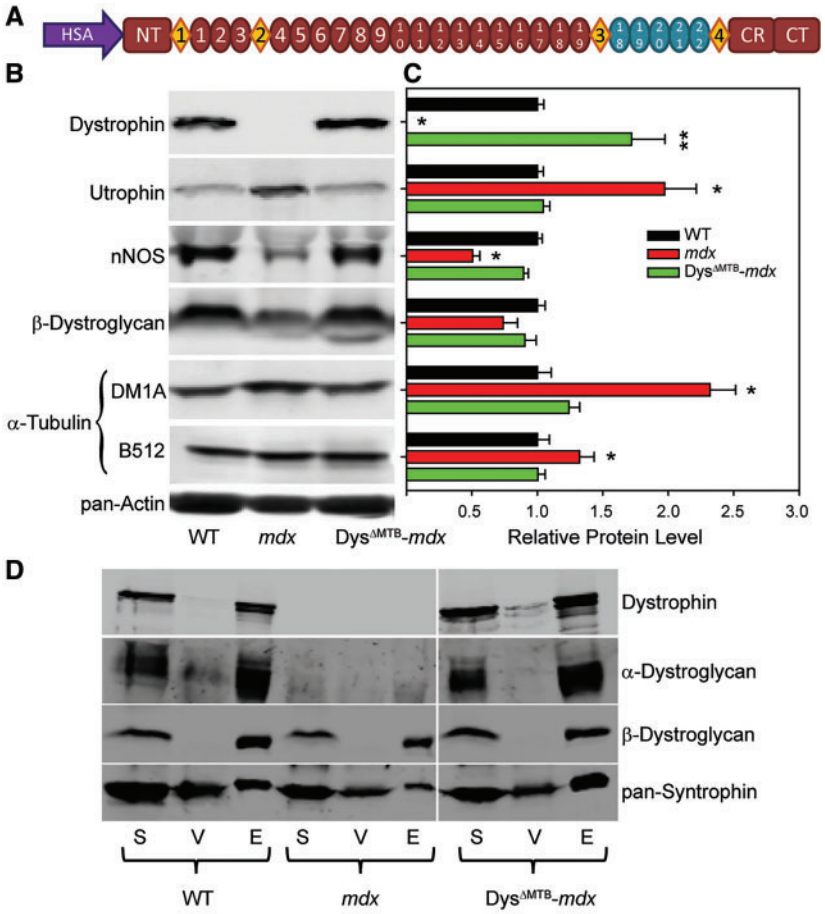

Figure 2. Generation of a transgenic mouse model expressing a dystrophin incapable of directly binding microtubules. (**A**) Constructs used to generate transgenic mice expressing a muscle-specific dystrophin incapable of binding microtubules. Ovals and diamonds are as in Figure 1. HSA, human skeletal α-actin promoter; NT, N-terminus; CR, cysteine rich domain; CT, C-terminus. (**B–C**) Dystrophin protein levels in Dys$^{\Delta MTB}$-*mdx* mice are ∼170% of WT levels. Utrophin and α-tubulin levels are elevated in *mdx* mice as compared with WT levels, but are restored to WT levels in the presence of transgenic dystrophin. nNOS and β-dystroglycan levels are reduced in *mdx* mice, but restored to WT levels in Dys$^{\Delta MTB}$-*mdx* mice. DM1A and B512 both recognize α-tubulin (see Materials and Methods), although DM1A shows a greater difference in immunoreactivity when probing *mdx* lysates than B512, as we previously reported (8). Sixty micrograms of quadriceps muscle lysate were run in each lane. Quantitation of protein levels is relative to pan-actin levels for all proteins. $n = 3$ mice per genotype. Statistics were carried out using one-way ANOVA with post-hoc *t*-test analyses with $P < 0.05$ considered significant *Statistically different from WT and Dys$^{\Delta MTB}$-*mdx*. **Statistically different from WT and *mdx*. (**D**) Transgenic dystrophin incorporates into the dystrophin–glycoprotein complex of Dys$^{\Delta MTB}$-*mdx* mice as evidenced by its presence in the elution fraction of the WGA enrichment. The dystroglycans and syntrophins are also present in the elution fraction. S, starting lysate; V, void fraction not bound to WGA beads; E, elution fraction from WGA beads.

passive muscle stiffness (9,29). In contrast, the Fiona-*mdx* mouse shows abnormal microtubule lattice organization and density (9), but WT levels of detyrosinated α-tubulin and desmin immunoreactivity (Fig. 6A and B), as well as WT passive muscle stiffness (Table 1).

Finally, we performed a microtubule fractionation analysis (30,31) to measure the proportion of detyrosinated α-tubulin immunoreactivity in free tubulin, free microtubules and membrane-associated microtubules (Fig. 6C). For all six mouse strains analyzed, the proportion of detyrosinated α-tubulin in each fraction was not different from the distribution of total α-tubulin. In addition, the distributions of detyrosinated α-tubulin were not significantly different among the different mouse strains. Our data demonstrate that *mdx*, Dys$^{\Delta 71\text{-}78}$-*mdx* and *Sgcb*$^{-/-}$ muscles all show increased levels of detyrosinated α-tubulin immunoreactivity that retains WT distribution within the different states of polymerization and membrane association.

Discussion

Here, we quantitatively compared a number of skeletal muscle microtubule perturbations associated with dystrophinopathy in mice across several transgenically rescued lines and with mice ablated for β-sarcoglycan (Table 2). Our principal findings are (1) that the microtubule-binding and microtubule-organizing functions of dystrophin are distinct and separable, (2) that sarcolemmal dystrophin expression is insufficient to maintain microtubule lattice organization in the face of at least one other perturbation to the dystrophin-glycoprotein complex (β-sarcoglycan deficiency) and (3) that elevated post-translational α-tubulin detyrosination does not directly correlate with subsarcolemmal microtubule density, lattice organization or rescue of nearly all skeletal muscle pathology in *mdx* mice by transgenic expression of nearly full-length dystrophin.

Our recent demonstration that utrophin lacks both microtubule binding and organizing activities (9) followed previous

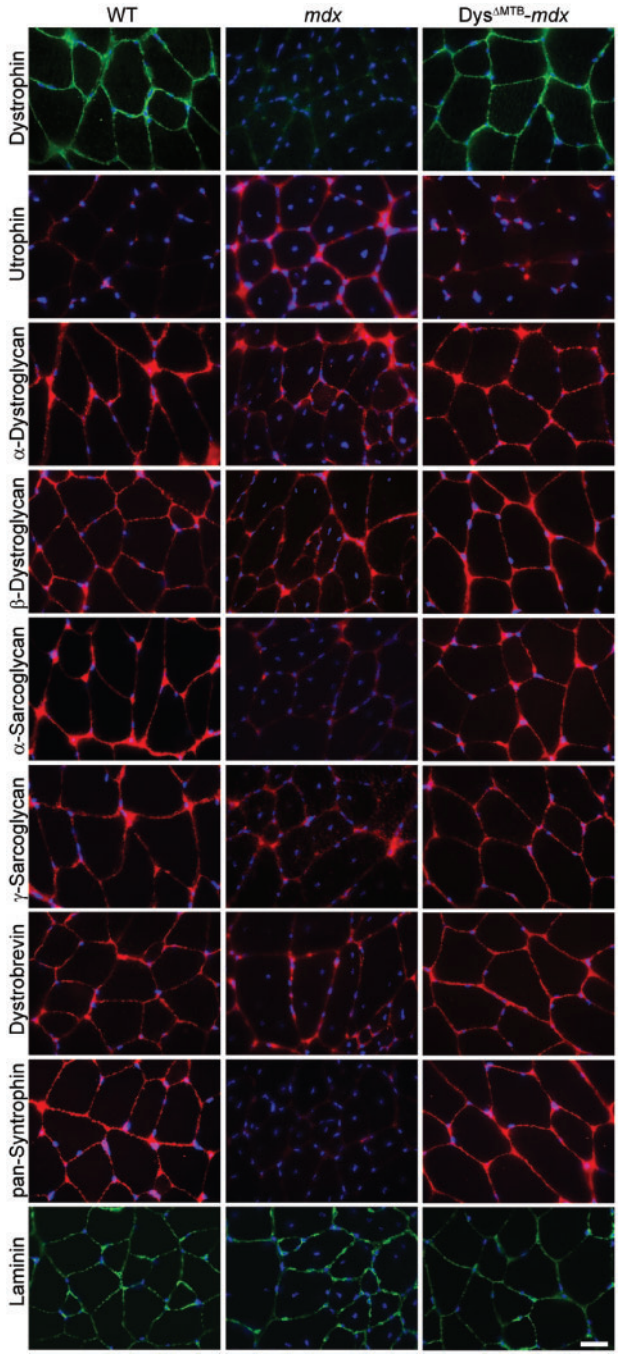

Figure 3. Restoration of the sarcolemmal dystrophin–glycoprotein complex in Dys$^{\Delta MTB}$-*mdx* mice. Dystrophin is absent in *mdx* mice. Utrophin levels are upregulated in *mdx* mice as compared with WT and Dys$^{\Delta MTB}$-*mdx* mice. Dys$^{\Delta MTB}$-*mdx* mice show presence of all dystrophin–glycoprotein complex components assayed at the sarcolemma. Bar, 20 μm.

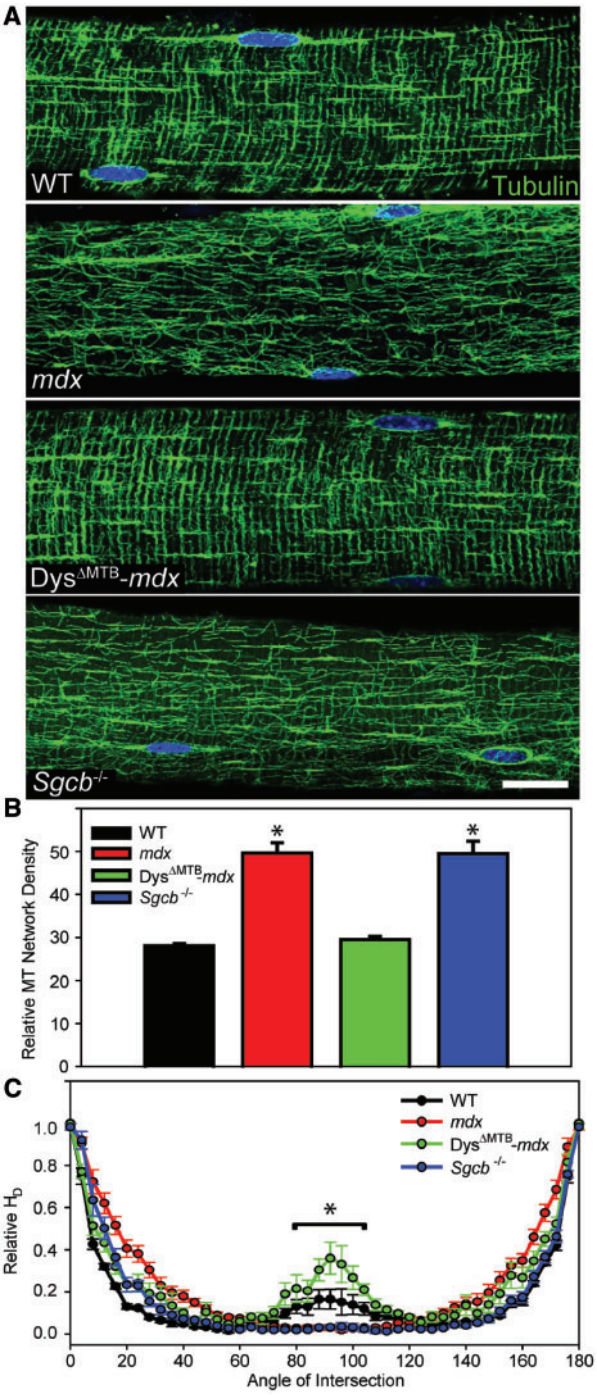

Figure 4. Rescue of subsarcolemmal microtubule lattice organization in Dys$^{\Delta MTB}$-*mdx* mice. (**A**) Microtubules are organized into a rectilinear lattice beneath the sarcolemma in WT and Dys$^{\Delta MTB}$-*mdx* mice in contrast to the perturbed microtubule lattice in *mdx* and *Sgcb*$^{-/-}$ mice. Images are representative of those obtained for $n \geq 10$ fibers from each of $n \geq 3$ mice per genotype. Bar, 20 μm. (**B**) WT and Dys$^{\Delta MTB}$-*mdx* mouse EDL fibers display the least dense microtubule network whereas *mdx* and *Sgcb*$^{-/-}$ mouse fibers display higher microtubule network density. *Statistically different from WT and Dys$^{\Delta MTB}$-*mdx*. (**C**) Transversely-oriented microtubules (centered around 90°) were significantly greater in WT and Dys$^{\Delta MTB}$-*mdx* mice compared with *mdx* and *Sgcb*$^{-/-}$ mice. Longitudinally oriented microtubules (0° and 180°) were not different between the mouse lines. Statistics were performed using one-way (density) or two-way (orientation) ANOVA with post-hoc *t*-test analyses with $P < 0.05$ considered significant. *WT and Dys$^{\Delta MTB}$-*mdx* mice are significantly different from *mdx* and *Sgcb*$^{-/-}$ between 80° and 100°.

work showing that utrophin is also incapable of localizing neuronal nitric oxide synthase (nNOS) to the sarcolemma (32,33). Our new results separating the *in vitro* microtubule binding and *in vivo* organizing activities of dystrophin parallel a study in which *in vitro* experiments identified the α1 helix of spectrin-like repeat 17 in sarcolemmal nNOS localization, but failed to detect critical *in vivo* contributions by the α2 and α3 helices of spectrin-like repeats 16 and 17, respectively (33). While the dystrophin N-terminal (ABD1) and middle rod (ABD2) actin binding

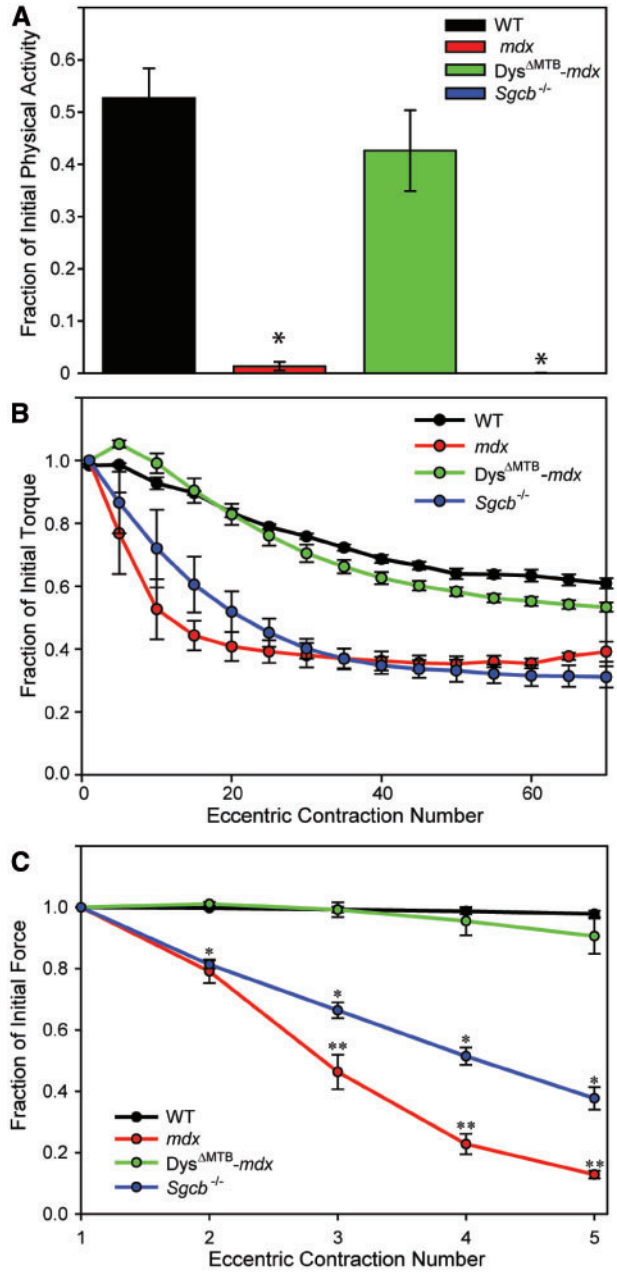

Figure 5. Normal skeletal muscle physiology in Dys$^{\Delta MTB}$-*mdx* mice. (**A**) Physical activity of mice immediately following mild treadmill exercise. WT and Dys$^{\Delta MTB}$-*mdx* mice exhibited ~40–50% of their initial cage activity after mild exercise whereas post-exercise activity in *mdx* and *Sgcb*$^{-/-}$ mice dropped >99% of their initial activity. $n \geq 4$ for each line. (**B**) As compared with WT and Dys$^{\Delta MTB}$-*mdx* mice, *mdx* and *Sgcb*$^{-/-}$ mice showed drastic loss of *in vivo* torque production of anterior crural muscles during a series of eccentric contractions. $n \geq 4$ for each line. (**C**) As compared with EDL muscles of WT and Dys$^{\Delta MTB}$-*mdx* mice, those of *mdx* mice show significant loss of *ex vivo* force after eccentric contraction. Isolated *Sgcb*$^{-/-}$ muscles also displayed significant loss of force after eccentric contraction, but not to the extent seen in *mdx* mice. $n \geq 4$ for each line. Statistics were performed using two-way ANOVA with post-hoc *t*-test analyses with $P < 0.05$ considered significant. *Statistically different from WT and Dys$^{\Delta MTB}$-*mdx* mice. **Statistically different from WT, Dys$^{\Delta MTB}$-*mdx* and *Sgcb*$^{-/-}$ mice. WT data were previously reported and shown here for comparison (9).

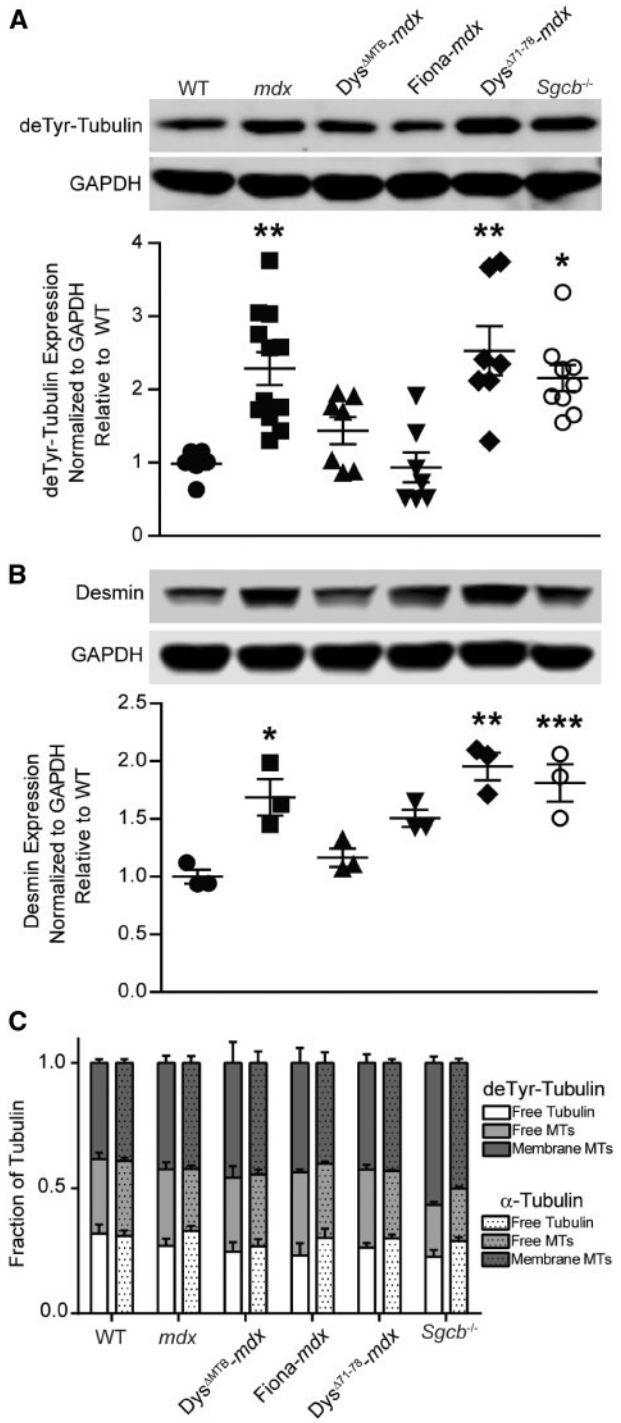

Figure 6. Analysis of cytoskeletal composition. (**A–B**). deTyr-tubulin (detyrosination of α-tubulin) and desmin levels are increased in *mdx*, Dys$^{\Delta 71\text{-}78}$-*mdx* and *Sgcb*$^{-/-}$ mice, but remain at WT levels in Dys$^{\Delta MTB}$-*mdx* and Fiona-*mdx* mice. $n \geq 3$ for each genotype. *$P < 0.05$, **$P < 0.01$, ***$P < 0.001$ as compared with WT. (**C**) Each tubulin fraction was blotted for total α-tubulin (DM1A) and deTyr-tubulin. $n \geq 3$ for each genotype. Proportions of each isoform in each fraction were plotted for each mouse strain and analyzed within each strain and between strains using ANOVA with post-hoc *t*-test analyses with $P < 0.05$ considered significant. No statistically significant differences were seen for any measured parameter.

Table 1. Physiological parameters of isolated EDL muscles used in *ex vivo* force measurements

	WT	*mdx*	Dys$^{\Delta MTB}$-*mdx*	*Sgcb*$^{-/-}$	*P* value
EDL mass (mg)	12.8 ± 0.4[a]	18.1 ± 0.7[b]	11.7 ± 0.2[c]	22.7 ± 0.4[b,c,d]	$P < 0.001$
L_0 (mm)	13.3 ± 0.2[a]	13.1 ± 0.2	12.2 ± 0.2[b,c]	13.6 ± 0.1[d]	$P = 0.003$
CSA (cm^2)	0.021 ± 0.001[a]	0.030 ± 0.001[b]	0.021 ± 0.001[c]	0.036 ± 0.001[b,c,d]	$P < 0.001$
Passive stiffness (N/m)	13.9 ± 0.9[a]	19.9 ± 0.8[b]	13.1 ± 1.3[c]	16.2 ± 1.2[b,c,d]	$P < 0.001$
P_0 (mN)	449 ± 8.8[a]	415 ± 12.8	424 ± 21.3	347 ± 25.0[b,c,d]	$P < 0.001$
Specific P_0 (N/cm^2)	21.8 ± 0.5[a]	14.1 ± 0.3[b]	20.6 ± 0.9[c]	9.7 ± 0.6[b,c,d]	$P < 0.001$
ΔP_0 (%)	11.1 ± 3.1[a]	86.7 ± 2.6[b]	11.0 ± 5.1[c]	80.9 ± 2.5[b,d]	$P < 0.001$
Force drop (%)	9.4 ± 5.7[a]	87.1 ± 1.3[b]	8.5 ± 2.3[c]	62.3 ± 3.0[b,c,d]	$P < 0.001$

Values are means ± SE.

L_0 = optimal muscle length, CSA = physiological cross sectional area, P_0 = maximal isometric tetanic force. ΔP_0 = change in P_0 after eccentric contractions. Force drop = change in eccentric force from the first to the fifth eccentric contraction. $n \geq 4$ for each line. Statistics were performed using two-way ANOVA with post-hoc t-test analyses with $P < 0.05$ considered significant.

[a]WT data were previously reported and shown here for comparison (9)

[b]Significantly different than WT.

[c]Significantly different than *mdx*.

[d]Significantly different than Dys$^{\Delta MTB}$-*mdx*.

domains first identified using *in vitro* assays (34,35) have been verified *in vivo* (36,37), subsequent *in vitro* experiments ascribing greater functional importance to the first calponin homology domain (CH1) of ABD1 (38) are less certain in light of the high *in vivo* functionality recently demonstrated for a dystrophin deleted for CH1 (39). Collectively, these results underscore the necessity to validate with *in vivo* experiments, dystrophin-related functions such as phospholipid binding that have so far been studied using only *in vitro* assays (e.g., 40). The possibility of species-dependent differences in dystrophic phenotype or phenotypic rescue (41) also reinforce the need to assess microtubule perturbations and associated pathological consequences in human DMD patients.

We also demonstrate that sarcolemmal dystrophin expression is not sufficient to organize the microtubule lattice, as evidenced by imaging data from skeletal muscle of the *Sgcb*$^{-/-}$ dystrophic mouse model. Clearly, dystrophin makes some unique contribution since transgenic expression of Dys$^{\Delta 71-78}$, but not utrophin, restores microtubule lattice organization to *mdx* muscle (9). Because the Dys$^{\Delta MTB}$-*mdx* mouse displays corrected microtubule lattice morphology and density in the absence of microtubule binding activity by Dys 20–24$_{Utr}$, we hypothesize that dystrophin may indirectly control subsarcolemmal microtubule lattice organization through one or more intermediary proteins. In support of this hypothesis, dystrophin is trafficked to the sarcolemma via interactions with the microtubule associated proteins ankyrin-B, β2-spectrin and dynactin-4, and its retention at the sarcolemma requires ankyrin-G (11,12). Moreover, proper localization of ankyrin-B to the sarcolemma relies on the giant scaffolding protein obscurin (13). Because the ankyrin-B/G binding site in dystrophin lies in close proximity to the binding site for β-dystroglycan (11), a challenge for future studies to map the microtubule organizing function of dystrophin will be to design *in vivo* screens that can perturb ankyrin binding without disrupting the critical interaction with β-dystroglycan binding.

While the exact pathophysiological consequences of microtubule derangement in skeletal muscle remain to be fully elucidated, recent work suggests that subsarcolemmal microtubule densification, disorganization and/or post-translational detyrosination contribute to pathology in the dystrophin-deficient *mdx* mouse (9,20,21,27). Specifically, eccentric contraction-induced force loss in dystrophin-deficient *mdx* muscle was ameliorated by microtubule depolymerization with colchicine (20), or by inhibition of α-tubulin detyrosination with the parthenolide prodrug dimethylamino-parthenolide (21). Our new data show that detyrosination of α-tubulin remains significantly elevated to *mdx* levels in Dys$^{\Delta 71-78}$-*mdx* mice that are rescued for virtually all other dystrophy phenotypes including eccentric contraction-induced force drop (Table 2 and ref. 9). The elevated α-tubulin detyrosination (Fig. 6A), desmin immunoreactivity (Fig. 6B), and passive stiffness values (Table 1 and ref. 9) shared by *mdx*, Dys$^{\Delta 71-78}$-*mdx* and *Sgcb*$^{-/-}$ muscle tempt speculation that these three parameters may be functionally linked. Such a link was recently demonstrated for the former two with cytoskeletal stiffness in cardiac muscle (27). Finally, our new data show that elevated α-tubulin detyrosination is separable and independent from the microtubule densification and disorganization that also manifest in dystrophin-deficient *mdx* muscle. Microtubule lattice derangement in *mdx* muscle correlates with reduced *in vivo* torque production after eccentric contraction in both *mdx* (9) and *Sgcb*$^{-/-}$ muscle (Fig. 5B). Thus, elucidating the causes of microtubule lattice density versus microtubule lattice disorganization and their contributions to the dystrophic phenotype will require new *in vivo* structure/function approaches.

Materials and Methods

Reagents

Anti-α-tubulin (DM1A, WB: 1:1000, IF: 1:200, epitope: amino acids 426-450), anti-α-tubulin (B512, 1:1000, epitope: C-terminal third), anti-pan-actin (C4, 1:5000), anti-Desmin (DE-U-10, 1:1000), anti-GAPDH (71.1, 1:10,000) and anti-laminin (L9393, 1:1000) antibodies were purchased from Sigma Aldrich. Anti-dystrophin (Dys2, 1:50), anti-β-dystroglycan (NCL-b-DG, 1:100), anti-α-sarcoglycan (NCL-a-SG, 1:100) and anti-γ-sarcoglycan (NCL-g-SG, 1:100) antibodies were purchased from Leica. Anti-utrophin (8A4, 1:50) antibody was purchased from Santa Cruz Biotechnology. Anti-α-dystroglycan (IIH6C4, WB: 1:500, IF: 1:100), anti-pan-syntrophin (1351, WB: 1:1000, IF: 1:100) and anti-deTyr-tubulin (AB3201, 1:500) antibodies were purchased from Millipore. An additional anti-deTyr-tubulin (1:10,000) antibody was previously described (42). Anti-dystrobrevin (23, 1:100) antibody was purchased from BD Biosciences. Anti-nNOS (Z-RNN3, 1:50) antibody, Alexa Fluor secondary antibodies (1:250)

Table 2. Summary of measured parameters across all mouse lines analyzed

	WT	*mdx*	Dys$^{\Delta MTB}$-*mdx*	Fiona-*mdx*	Dys$^{\Delta 71\text{-}78}$-*mdx*	*Sgcb*$^{-/-}$
MT density	WT[a]	↑[a]	WT	↑[a]	WT[a]	↑
MT organization	WT[a]	↓[a]	WT	↓[a]	WT[a]	↓
In vivo ECC torque loss	WT[a]	↑[a]	WT	↑[a]	WT[a]	↑
Passive stiffness	WT[a]	↑[a]	WT	WT[a]	↑[a]	↑
deTyr-Tubulin	WT	↑	WT	WT	↑	↑
Desmin	WT	↑	WT	WT	↑	↑
Dystrophic pathology	No	Yes	No	No[b]	No[c]	Yes[d]

Up arrows indicate a significant increase above WT values, down arrows indicate a significant decrease below WT values.

[a]Data previously measured using the exact methods employed in this study and shown for comparison (9).

[b]Previously reported (28).

[c]Previously reported (29).

[d]Previously reported (24).

and Alexa Fluor α-bungarotoxin (1:500) were purchased from Invitrogen. DyLight 680 and 800 secondary antibodies (1:10,000) were purchased from Pierce. Wheat germ agglutinin agarose beads were purchased from Vector Laboratories. Pre-formed microtubules and paclitaxel were purchased from Cytoskeleton. DNA primers were purchased from Integrated DNA Technologies.

Cloning

All dystrophin and utrophin plasmid constructs were PCR-amplified from existing N-terminally FLAG-tagged pFastBac1 constructs generated in our previous studies (8,9,43–46), inserted into the Gateway entry vector pENTR/D-TOPO (Invitrogen) and sequence verified. All PCRs were performed using PfuII Ultra HS polymerase (Stratagene). Once verified, entry vectors were recombined into the Gateway insect cell destination vector, pDEST8, using LR Clonase II (Invitrogen) and subsequently expressed in Sf9 insect cells using the Bac-to-Bac system (Invitrogen). Deletion constructs were built as previously described (47). In brief, PCR primers were designed such that they amplified the entire plasmid except the deleted region. The linear PCR products were circularized via the addition of T4 polynucleotide kinase and T4 DNA ligase (New England Biolabs) and sequence verified. To generate dystrophin/utrophin hybrid constructs, PCR primers were designed to amplify the entire dystrophin plasmid except the repeats to be exchanged with primers containing 15 nucleotide overhangs homologous to the ends of the utrophin repeats chosen for substitution. In addition, the homologous utrophin repeats for substitution were PCR amplified with primers containing 15 nucleotide overhangs homologous to the dystrophin repeat sequences flanking the hybrid region. The two resulting PCR products were mixed in equimolar ratios and assembled into a single vector using the Gibson Assembly Master Mix (New England Biolabs).

Protein expression and purification

FLAG-tagged dystrophin and utrophin proteins were expressed and purified in Sf9 insect cells using the Bac-to-Bac protocol (Invitrogen). In brief, recombinant baculoviral DNA was transfected into a small culture of Sf9 insect cells using CellFectin II (Invitrogen). Four days later, the media containing the recombinant baculovirus was harvested and the transfected cells were analyzed for protein expression by anti-FLAG western blot. Once expression was verified, large cultures were incubated for 3 days with amplified baculovirus before being harvested for protein purification. For purification, cells were lysed using 1% Triton in phosphate buffered saline (PBS: 8 mM NaH_2PO_4, 42 mM Na_2HPO_4, 150 mM NaCl, pH 7.5) containing protease inhibitors (100 nM aprotinin, 1 mM benzamidine, 10 μM E-64, 10 μM leupeptin, 1 mM pepstatin A and 1 mM phenylmethanesulfonylfluoride) and protein purified using M2 FLAG affinity agarose (Sigma) as previously described (8,45,46). Proteins were dialyzed into microtubule buffer (50 mM HEPES, 50 mM KCl, 1 mM $MgCl_2$, 1 mM EGTA, pH 7.5) overnight at 4°C before being concentrated and used in *in vitro* microtubule cosedimentation assays.

Mice

All animals were housed and treated in accordance with the standards set by the University of Minnesota Institutional Animal Care and Use Committee. WT mice used in this study were C57BL/10 obtained from Jackson Laboratories. Congenic Fiona-*mdx*, Dys$^{\Delta 71–78}$-*mdx* and Dys$^{\Delta MTB}$-*mdx* were bred for at least ten generations onto the *mdx* (C57BL/10ScSn-*Dmd*^{mdx}/J) mouse strain obtained from Jackson Laboratories. *Sgcb*$^{-/-}$ mice were originally obtained from Jackson Laboratories (B6.129-*Sgcb*^{tm1Kcam}/1J) and backcrossed onto C57BL/6 mice. All mice used in this study were male.

Generation of transgenic mice

The HSA promoter was cloned in place of the cytomegalovirus promoter in the Gateway version of the mammalian expression vector pcDNA, pDEST40. This new plasmid (pDEST-HSA) was used to create a transgene with the Dys R20–24$_{Utr}$ construct, built in the pENTR/D-TOPO vector for *in vitro* binding studies as described above. pDEST-HSA-Dys R20–24$_{Utr}$ DNA was restriction digested to linearize the transgene, gel extracted, and sent to the Mouse Genetics Core at The Scripps Research Institute for pronuclear injection into C57BL/6J mice. Transgenic founder mice were identified by PCR using HSA-specific primers (Forward: 5′-GTC AGG AGG GGC AAA CCC GC-3′, Reverse: 5′-GTC GCT GCC CTT CTC GAG CC-3′, Product Size: 187 bp) and crossed with C57BL/10 mice to check for transgene transmission. Transgenic dystrophin protein expression was assessed in several different muscles from each transgenic line crossed onto the *mdx* (C57BL/10ScSn-*Dmd*^{mdx}/J) background using

quantitative western blotting. All Dys$^{\Delta MTB}$-*mdx* mice used in this study were compared with non-transgenic littermate *mdx* mice as controls.

Biochemical characterization of the dystrophin-glycoprotein complex

Quadriceps muscle tissue was harvested from each mouse line, snap frozen in liquid nitrogen, ground with a mortar and pestle and lysed for 30 min in 1% Triton in PBS containing protease inhibitors. Lysates were clarified by centrifugation, an aliquot collected as a starting lysate sample, and the remaining lysate incubated with wheat germ agglutinin conjugated agarose beads overnight at 4°C while rotating. The next day, the lysate was removed from the beads and kept as the void fraction. The beads were washed three times with 0.1% Triton in PBS. After washing, the beads were boiled in 2× Laemmli sample buffer (5% sodium dodecyl sulfate, 192 mM sucrose, 108 mM Tris, 710 mM β-mercaptoethanol, 0.0007% bromophenol blue) for 5 min. This fraction was taken as the elution. Equivalent volumes from each fraction were run side-by-side.

Immunofluorescence

Quadriceps muscles from each mouse line were cryopreserved in OCT and 10 μm transverse sections cut. Sections were fixed in 4% paraformaldehyde in PBS for 10 min and subsequently washed three times in PBS with 0.1% Triton for 5 min each. Primary antibodies were incubated overnight at 4°C in a humidified chamber. The next day, slides were washed three times in PBS with 0.1% Triton for 5 min each and goat anti-mouse or anti-rabbit secondary antibody coupled to Alexa Fluor 488 or 568 was incubated on the sections for 30 min at 37°C. Sections were washed three times in PBS with 0.1% Triton for 5 min each and slides sealed using SlowFade Gold antifade reagent with DAPI to visualize nuclei. Images were acquired on a Deltavision PersonalDV deconvolution microscope equipped with a 40× 1.35 NA oil objective.

Neuromuscular junction imaging

Gastrocnemius muscles from each mouse line were cryopreserved in OCT and 20 μm longitudinal sections cut. Sections were fixed in 4% paraformaldehyde in PBS for 10 min and subsequently washed three times in PBS for 5 min each. Alexa Fluor 488-conjugated α-bungarotoxin was incubated on the sections for 30 min at 37°C. Sections were washed three times in PBS for 5 min each and slides sealed using SlowFade Gold antifade reagent with DAPI to visualize nuclei. Images were acquired on a Deltavision PersonalDV deconvolution microscope equipped with a 100× 1.40 NA oil objective.

Ex vivo EDL force measurements

EDL muscles of 6-month-old mice were passively shortened to 95% resting length and then stimulated for 200 ms while the muscle was simultaneously lengthened to 105% resting length at 0.5 length/s. To prevent fatigue, each eccentric contraction was separated by 3 min of rest. Force production was plotted as a percentage of initial force.

In vivo muscle torque measurements

In brief, torque about the ankle joint of 12-week-old mice was measured for each eccentric contraction and plotted as a fraction of the first eccentric contraction. To prevent fatigue, each eccentric contraction was separated by 3 min of rest.

Exercise-induced inactivity

In brief, prior to activity cage assessments, 10-week-old mice were acclimated to the treadmill for three consecutive days. On the fourth day, baseline voluntary activity was assessed for 30 min prior to exercise using activity cages (AccuScan Instruments Inc.). Mice were then placed on the treadmill set at 15° decline. Without the use of electrical shock, mice were encouraged to walk for 5 min at 5 m/min followed by 10 min at 15 m/min. After exercise, mice were placed back in the same activity cages and activity monitored for 30 min after exercise. Data were plotted as to represent the percentage of pre-exercise activity the mice retained after exercise.

Tubulin fractionation

Tubulin fractionation was performed as previously described (30,31). In brief, quadriceps muscle from each mouse strain analyzed was snap frozen in liquid nitrogen and ground into a fine powder using a mortar and pestle. The tissue was then lysed in MT stabilization buffer (10 mM sodium phosphate, 0.5 mM EGTA, 0.5 mM GTP, 0.5 mM $MgCl_2$, 50% glycerol (v/v), 5% DMSO (v/v) and protease inhibitors, pH 6.95). The solution was centrifuged at 100,000 *g* for 20 min at room temperature and the supernatant taken as *Free Tubulin*. The pellet was dissolved in MT destabilization buffer (250 mM sucrose, 10 mM sodium phosphate, 0.5 mM GTP, 0.5 mM $MgCl_2$ and protease inhibitors, pH 6.95) for 2 h on ice. After centrifugation for 20 min at 4°C, the supernatant was taken as *Free MTs*. The pellet was dissolved on ice for 10 min in Triton lysis buffer (20 mM Tris–HCL, 150 mM NaCl, 1 mM EDTA, 10% glycerol (v/v), 1% Triton-X100 (v/v) and protease inhibitors, pH 7.5), centrifuged at 14,000 *g* for 10 min at 4°C and the supernatant taken as *Membrane MTs*. The last steps to isolate the *Membrane MTs* were repeated once more to increase the yield. The remaining pellet contained insoluble cytoskeletal proteins and was discarded after verifying the absence of tubulin in the fraction.

Additional methods

EDL muscle fiber imaging and quantitation were all performed exactly as previously described (9,48). *In vitro* microtubule cosedimentation assays were performed as previously described (9). Additional information on *ex vivo* EDL force measurements, *in vivo* anterior crural muscle torque measurements, and mouse activity cage measurements was previously described (9).

Supplementary Material

Supplementary Material is available at *HMG* online.

Acknowledgements

The authors would like to thank Drs. Wenhua Liu and Evelyn Ralston (National Institute of Arthritis and Musculoskeletal and Skin Diseases) for providing the directionality analysis program

and Dr. DeWayne Townsend (University of Minnesota) for a breeding pair of *Sgcb*$^{-/-}$ mice.

Conflict of Interest statement. None declared

Funding

The study was supported by National Institute of Arthritis and Musculoskeletal and Skin Diseases grant to J.M.E. [RO1 AR042423]. J.J.B. and J.T.O. were supported by the National Institutes of Health Training Program in Muscle Research [AR007612]. J.J.B. was also supported by a University of Minnesota Doctoral Dissertation Fellowship. J.T.O., T.L.M. and D.M.N. were each supported by fellowships from the National Institute on Aging Training Program for Functional Proteomics of Aging [T32 AG029796]. D.M.T. was supported by an American Heart Association Predoctoral Fellowship [12PRE12040402].

References

1. Hoffman, E.P., Brown, R.H. and Kunkel, L.M. (1992) Dystrophin: the protein product of the Duchene muscular dystrophy locus. *Biotechnology*, **24**, 457–466.
2. Worton, R.G. and Thompson, M.W. (1988) Genetics of Duchenne muscular dystrophy. *Annu. Rev. Genet.*, **22**, 601–629.
3. Mendell, J.R., Shilling, C., Leslie, N.D., Flanigan, K.M., Al-Dahhak, R., Gastier-Foster, J., Kneile, K., Dunn, D.M., Duval, B., Aoyagi, A., *et al.* (2012) Evidence-based path to newborn screening for Duchenne muscular dystrophy. *Ann. Neurol.*, **71**, 304–313.
4. Rall, S. and Grimm, T. (2012) Survival in Duchenne muscular dystrophy. *Acta Myol.*, **31**, 117–120.
5. Angelini, C. (2007) The role of corticosteroids in muscular dystrophy: a critical appraisal. *Muscle Nerve*, **36**, 424–435.
6. Ricotti, V., Ridout, D.A., Scott, E., Quinlivan, R., Robb, S.A., Manzur, A.Y. and Muntoni, F. (2013) Long-term benefits and adverse effects of intermittent versus daily glucocorticoids in boys with Duchenne muscular dystrophy. *J. Neurol. Neurosurg. Psychiatry*, **84**, 698–705.
7. Ervasti, J.M. (2003) Costameres: The Achilles' heel of Herculean muscle. *J. Biol. Chem.*, **278**, 13591–13594.
8. Prins, K.W., Humston, J.L., Mehta, A., Tate, V., Ralston, E. and Ervasti, J.M. (2009) Dystrophin is a microtubule-associated protein. *J. Cell Biol.*, **186**, 363–369.
9. Belanto, J.J., Mader, T.L., Eckhoff, M.D., Strandjord, D.M., Banks, G.B., Gardner, M.K., Lowe, D.A. and Ervasti, J.M. (2014) Microtubule binding distinguishes dystrophin from utrophin. *Proc. Natl. Acad. Sci. U. S. A.*, **111**, 5723–5728.
10. Percival, J.M., Gregorevic, P., Odom, G.L., Banks, G.B., Chamberlain, J.S. and Froehner, S.C. (2007) rAAV6-Microdystrophin rescues aberrant Golgi complex organization in mdx skeletal muscles. *Traffic*, **8**, 1424–1439.
11. Ayalon, G., Davis, J.Q., Scotland, P.B. and Bennett, V. (2008) An Ankyrin-based mechanism for functional organization of dystrophin and dystroglycan. *Cell*, **135**, 1189–1200.
12. Ayalon, G., Hostettler, J.D., Hoffman, J., Kizhatil, K., Davis, J.Q. and Bennett, V. (2011) Ankyrin-B interactions with spectrin and dynactin-4 are required for dystrophin-based protection of skeletal muscle from exercise injury. *J. Biol. Chem.*, **286**, 7370–7378.
13. Randazzo, D., Giacomello, E., Lorenzini, S., Rossi, D., Pierantozzi, E., Blaauw, B., Reggiani, C., Lange, S., Peter, A.K., Chen, J., *et al.* (2013) Obscurin is required for ankyrinB-dependent dystrophin localization and sarcolemma integrity. *J. Cell Biol.*, **200**, 523–536.
14. Saitoh, O., Arai, T. and Obinata, T. (1988) Distribution of microtubules and other cytoskeletal filaments during myotube elongation as revealed by fluorescence microscopy. *Cell Tissue Res.*, **252**, 263–273.
15. Chang, W., Webster, D.R., Salam, A.A., Gruber, D., Prasad, A., Eiserich, J.P. and Bulinski, J.C. (2002) Alteration of the C-terminal amino acid of tubulin specifically inhibits myogenic differentiation. *J. Biol. Chem.*, **277**, 30690–30698.
16. Perez, O.D., Chang, Y.T., Rosania, G., Sutherlin, D. and Schultz, P.G. (2002) Inhibition and reversal of myogenic differentiation by purine-based microtubule assembly inhibitors. *Chem. Biol.*, **9**, 475–483.
17. Ralston, E., Lu, Z. and Ploug, T. (1999) The organization of the Golgi complex and microtubules in skeletal muscle is fiber type-dependent. *J. Neurosci.*, **19**, 10694–10705.
18. Ralston, E., Ploug, T., Kalhovde, J. and Lomo, T. (2001) Golgi complex, endoplasmic reticulum exit sites, and microtubules in skeletal muscle fibers are organized by patterned activity. *J. Neurosci.*, **21**, 875–883.
19. Prosser, B.L., Ward, C.W. and Lederer, W.J. (2011) X-ROS signaling: rapid mechano-chemo transduction in heart. *Science*, **333**, 1440–1445.
20. Khairallah, R.J., Shi, G., Sbrana, F., Prosser, B.L., Borroto, C., Mazaitis, M.J., Hoffman, E.P., Mahurkar, A., Sachs, F., Sun, Y., *et al.* (2012) Microtubules underlie dysfunction in Duchenne muscular dystrophy. *Sci. Signal*, **5**, ra56.
21. Kerr, J.P., Robison, P., Shi, G., Bogush, A.I., Kempema, A.M., Hexum, J.K., Becerra, N., Harki, D.A., Martin, S.S., Raiteri, R., *et al.* (2015) Detyrosinated microtubules modulate mechanotransduction in heart and skeletal muscle. *Nat. Commun.*, **6**, 8526.
22. Matsumura, K., Ervasti, J.M., Ohlendieck, K., Kahl, S.D. and Campbell, K.P. (1992) Association of dystrophin-related protein with dystrophin-associated proteins in mdx mouse muscle. *Nature*, **360**, 588–591.
23. Araishi, K., Sasaoka, T., Imamura, M., Noguchi, S., Hama, H., Wakabayashi, E., Yoshida, M., Hori, T. and Ozawa, E. (1999) Loss of the sarcoglycan complex and sarcospan leads to muscular dystrophy in β-sarcoglycan-deficient mice. *Hum. Mol. Genet.*, **8**, 1589–1598.
24. Durbeej, M., Cohn, R.D., Hrstka, R.F., Moore, S.A., Allamand, V., Davidson, B.L., Williamson, R.A. and Campbell, K.P. (2000) Disruption of the β-Sarcoglycan gene reveals pathogenetic complexity of limb-girdle muscular dystrophy type 2E. *Mol. Cell*, **5**, 141–151.
25. Kobayashi, Y.M., Rader, E.P., Crawford, R.W., Iyengar, N.K., Thedens, D.R., Faulkner, J. A., Parikh, S.V., Weiss, R.M., Chamberlain, J.S., Moore, S. a., *et al.* (2008) Sarcolemma-localized nNOS is required to maintain activity after mild exercise. *Nature*, **456**, 511–515.
26. Petrof, B.J., Shrager, J.B., Stedman, H.H., Kelly, A. M. and Sweeney, H.L. (1993) Dystrophin protects the sarcolemma from stresses developed during muscle contraction. *Proc. Natl Acad. Sci. U. S. A.*, **90**, 3710–3714.
27. Robison, P., Caporizzo, M.A., Ahmadzadeh, H., Bogush, A.I., Chen, C.Y., Margulies, K.B., Shenoy, V.B. and Prosser, B.L. (2016) Detyrosinated microtubules buckle and bear load in contracting cardiomyocytes. *Science*, **352**, aaf0659.
28. Tinsley, J., Deconinck, N., Fisher, R., Kahn, D., Phelps, S., Gillis, J.M. and Davies, K. (1998) Expression of full-length utrophin prevents muscular dystrophy in mdx mice. *Nat. Med.*, **4**, 1441–1444.

29. Crawford, G.E., Faulkner, J.A., Crosbie, R.H., Campbell, K.P., Froehner, S.C. and Chamberlain, J.S. (2000) Assembly of the dystrophin-associated protein complex does not require the dystrophin COOH-terminal domain. *J. Cell Biol.*, **150**, 1399–1409.
30. Ostlund, R.E., Leung, J.T. and Hajek, S.V. (1979) Biochemical determination of tubulin-microtubule equilibrium in cultured cells. *Anal. Biochem.*, **96**, 155–164.
31. Fassett, J.T., Xu, X., Kwak, D., Wang, H., Liu, X., Hu, X., Bache, R.J. and Chen, Y. (2013) Microtubule actin cross-linking factor 1 regulates cardiomyocyte microtubule distribution and adaptation to hemodynamic overload. *PLoS One*, **8**, 1–12.
32. Li, D., Bareja, A., Judge, L., Yue, Y., Lai, Y., Fairclough, R., Davies, K.E., Chamberlain, J.S. and Duan, D. (2010) Sarcolemmal nNOS anchoring reveals a qualitative difference between dystrophin and utrophin. *J. Cell Sci.*, **123**, 2008–2013.
33. Lai, Y., Zhao, J., Yue, Y. and Duan, D. (2013) α2 and α3 helices of dystrophin R16 and R17 frame a microdomain in the α1 helix of dystrophin R17 for neuronal NOS binding. *Proc. Natl Acad. Sci. U. S. A.*, **110**, 525–530.
34. Way, M., Pope, B., Cross, R.A., Kendrick-Jones, J. and Weeds, A.G. (1992) Expression of the N-terminal domain of dystrophin in *E. coli* and demonstration of binding to F-actin. *FEBS Lett.*, **301**, 243–245.
35. Rybakova, I.N., Amann, K.J. and Ervasti, J.M. (1996) A new model for the interaction of dystrophin with F-actin. *J. Cell Biol.*, **135**, 661–672.
36. Warner, L.E., DelloRusso, C., Crawford, R.W., Rybakova, I.N., Patel, J.R., Ervasti, J.M. and Chamberlain, J.S. (2002) Expression of Dp260 in muscle tethers the actin cytoskeleton to the dystrophin-glycoprotein complex and partially prevents dystrophy. *Hum. Mol. Genet.*, **11**, 1095–1105.
37. Hanft, L.M., Rybakova, I.N., Patel, J.R., Rafael-Fortney, J.A. and Ervasti, J.M. (2006) Cytoplasmic gamma-actin contributes to a compensatory remodeling response in dystrophin-deficient muscle. *Proc. Natl Acad. Sci. U. S. A.*, **103**, 5385–5390.
38. Singh, S.M., Bandi, S., Winder, S.J. and Mallela, K.M.G. (2014) The actin binding affinity of the utrophin tandem calponin-homology domain is primarily determined by its N-terminal domain. *Biochemistry*, **53**, 1801–1809.
39. Wein, N., Vulin, A., Falzarano, M.S., Szigyarto, C.A.K., Maiti, B., Findlay, A., Heller, K.N., Uhlén, M., Bakthavachalu, B., Messina, S., *et al.* (2014) Translation from a DMD exon 5 IRES results in a functional dystrophin isoform that attenuates dystrophinopathy in humans and mice. *Nat. Med.*, **20**, 992–1000.
40. Sarkis, J., Vie, V., Winder, S.J., Renault, A., Le Rumeur, E. and Hubert, J.F. (2013) Resisting sarcolemmal rupture: dystrophin repeats increase membrane-actin stiffness. *FASEB J*, **27**, 359–367.
41. Wang, B., Li, J., Qiao, C., Chen, C., Hu, P., Zhu, X., Zhou, L., Bogan, J., Kornegay, J. and Xiao, X. (2008) A canine minidystrophin is functional and therapeutic in mdx mice. *Gene Ther.*, **15**, 1099–1106.
42. Gundersen, G.G., Kalnoski, M.H. and Bulinski, J.C. (1984) Distinct populations of microtubules: tyrosinated and nontyrosinated alpha tubulin are distributed differently in vivo. *Cell*, **38**, 779–789.
43. Poirier, M.G., Eroglu, S. and Marko, J.F. (2002) The bending rigidity of mitotic chromosomes. *Mol. Biol. Cell*, **13**, 2170–2179.
44. Rybakova, I.N., Humston, J.L., Sonnemann, K.J. and Ervasti, J.M. (2006) Dystrophin and utrophin bind actin through distinct modes of contact. *J. Biol. Chem.*, **281**, 9996–10001.
45. Henderson, D.M., Lee, A. and Ervasti, J.M. (2010) Disease-causing missense mutations in actin binding domain 1 of dystrophin induce thermodynamic instability and protein aggregation. *Proc. Natl Acad. Sci. U. S. A.*, **107**, 9632–9637.
46. Henderson, D.M., Belanto, J.J., Li, B., Heun-Johnson, H. and Ervasti, J.M. (2011) Internal deletion compromises the stability of dystrophin. *Hum. Mol. Genet.*, **20**, 2955–2963.
47. Imai, Y., Matsushima, Y., Sugimura, T. and Terada, M. (1991) A simple and rapid method for generating a deletion by PCR. *Nucleic Acids Res.*, **19**, 2785.
48. Liu, W. and Ralston, E. (2014) A new directionality tool for assessing microtubule pattern alterations. *Cytoskeleton*, **71**, 230–240.